Source Seeking With Very Slow or Drifting Sensors

Nima Ghods[1]
e-mail: nimaghods@gmail.com

Miroslav Krstic
e-mail: krstic@ucsd.edu

Department of Mechanical and Aerospace Engineering,
University of California, San Diego,
La Jolla, CA 92093-0411

Slow sensors arise in many applications, including sensing chemical concentrations in tracking of contaminant plumes. Slow sensors are often the cause of poor performance and a potential cause of instability. In this paper, we design a modified extremum seeking scheme to account and exploit slow sensor dynamics. We also consider the worst case, which is sensor dynamics governed by a pure integrator. We provide stability results for several distinct variations of an extremum seeking scheme for one-dimensional optimization. Then we develop a design for source seeking in a plane using a fully actuated vehicle, prove its closed-loop convergence, and present simulation results. We use metal oxide microhotplate gas sensors as a real world example of slow sensor dynamics, model the sensor based on experimental data, and employ the identified sensor model in our source seeking simulations. [DOI: 10.1115/1.4003639]

1 Introduction

Recent advances in extremum seeking have shown it to be a powerful tool in real time nonmodel based control and optimization [1–6]. Success has been achieved in compensating slow actuator dynamics [7–9], but no results have been reported on extremum seeking for plants with slow sensor dynamics or in the extreme case of sensors governed by a pure integrator (drifting sensors). In this paper, we introduce a new idea of how to extend extremum seeking to deal with a slow or drifting sensor.

For simplicity, we first consider a single-parameter extremum seeking problem with a static map and sensor dynamics. Then we consider a 2D problem with simple vehicle dynamics and with slow sensor dynamics. The classical extremum seeking scheme [10] is modified by observing that the integrator, a key adaptation element, is already present in the sensor dynamics, if they are governed by a pure integrator. We perform an appropriate (time-varying) swap of the integrator block and the demodulation block (Sec. 3), and as a result obtain a scheme where the map output converges to the extremum fast, while the sensor output may converge slowly, or it may even drift to infinity. Stability and simulation results are presented first for a system with a slow sensor (Sec. 4). This is followed by the results for a sensor governed by a pure integrator (Sec. 5). (These results do not imply one another.) Finally, results for the case of a 2D point mass vehicle with a slow sensor are presented (Sec. 6).

Traditional methods for gas plume seeking using slow metal oxide sensors [11–13] (reviewed in Sec. 2) either wait for a big enough change in the sensor reading or for the sensor reading to settle before they act. Most of these search methods [14–16] are based on mimicking insect behavior (mainly moths) to localize source of odor without much consideration of the sensor dynamics. The modified extremum seeking (ES) scheme reacts to the sensor reading continuously, which allows the overall system to converge to an optimum much faster than the sensor settling time.

Our compensation of slow sensor dynamics does *not* amount to employing a differentiator after the sensor to cancel the integrator in the sensor and act on the trend of the signal, rather than on the value of the signal. This approach would result in amplification of noise. Instead, our approach *leverages* the integrator action in the sensor, to have it assume the role of the tuning element in the extremum seeking loop. We highlight this by considering both a version of the modified scheme with the standard washout filter in the loop and a version without the washout filter, proving stability in each case.

To show the capabilities of the modified extremum seeking scheme with the metal oxide sensors, we consider the realistic two dimensional problem of trying to localize a gas leak in a room with a single moving sensor. In the 2D source seeking problem, we are faced with the problem that two integrators exist in the loop, one from the sensor and one associated with the vehicle model. A modification of the extremum seeking scheme is needed to reduce the loop phase drop from 180 deg to a lesser value. This modification comes in the form of a washout filter to approximate differentiator, or, if preferred, in the form of a phase-lead compensator.

2 Model of a Metal Oxide Sensor

Due to their small size, metal oxide based microhotplate sensors can be used to develop a portable, sensitive, and low-cost gas monitoring system to detect, for example, leakage of hazardous gases. Modeling metal oxide microhotplate sensor dynamics accurately can prove to be very difficult, as seen in Refs. [17–19]. In this section, we make a reasonable assumption to simplify the complicated models. The basic premise of the sensor model in Refs. [17–19] is that the sensor reading is driven by an exponential of the concentration of several gases, and the gas concentrations are governed by several coupled ordinary differential equations (ODEs), which correspond chemical reactions. To better understand the sensor dynamics, the metal oxide sensor was exposed to different concentrations of ethanol shown in Fig. 1(*a*).

From these tests, we see that the dominant dynamics of the sensor are governed by a first order system

$$G_{\text{sensor}}(s) = \frac{b}{s+\varepsilon} \tag{1}$$

where b and ε are the positive constants that depend on the sensor and the type of gases. After performing several tests, we observed that, although ε is positive, its magnitude is quite small (on the order of 10^{-2}). By inspection, we set $b=0.037$ and $\varepsilon=0.046$ to get the model for the gas sensor reacting to ethanol. Figure 1(*b*) compares the identified sensor model against the real TGS2602 gas sensor reading. The sensor model parameters change for different gases and different sensors but always stay positive.

3 Extremum Seeking Design for Slow Sensors

In this section, we modify the classical extremum seeking scheme to work with very slow sensors. In the extreme case, the sensors are governed by a pure integrator, namely, drifting sensors. We start with a key observation that an integrator is already a part of the classical extremum seeking loop in Fig. 2(*a*). We need to modify the scheme so that the sensor itself is performing the task of this integrator. To do this, we need to swap the integrator and the multiplication by $\sin(\omega t)$ in Fig. 2(*a*), i.e., to move the integrator upstream in the signal path. This is not a simple swap of linear blocks because a *multiplication* by a time varying signal is involved. However, using integration by parts, we get that $\int_0^t \eta(\tau)\sin(\omega\tau)\mathrm{d}\tau = \sin(\omega t)\int_0^t \eta(\tau)\mathrm{d}\tau - \omega\int_0^t \cos(\omega\tau)\int_0^\tau \eta(\sigma)\mathrm{d}\sigma\mathrm{d}\tau$.

[1]Corresponding author.

Contributed by the Dynamic Systems Division of ASME for publication in the Journal of Dynamic Systems, Measurement, and Control. Manuscript received December 16, 2008; final manuscript received October 28, 2010; published online April 11, 2011. Assoc. Editor: Guoming George Zhu.

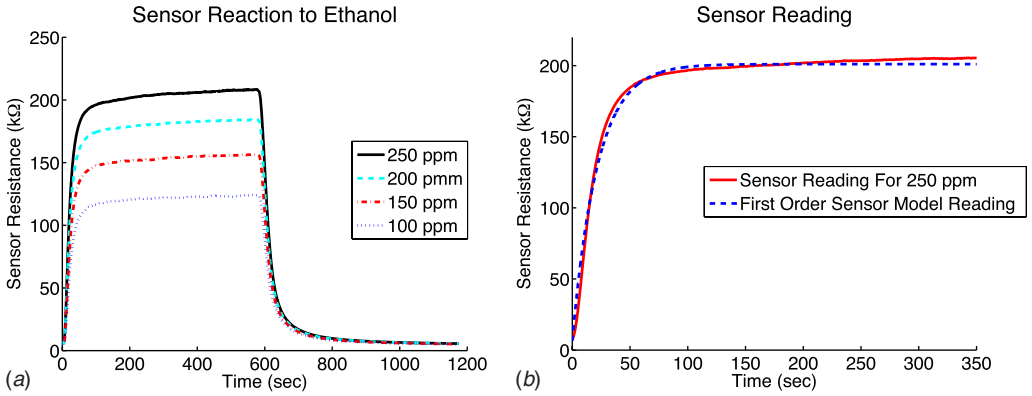

Fig. 1 (*a*) An example of metal oxide sensor TGS2602 responding to four different concentrations of ethanol. (*b*) Comparison of the first order sensor model and the real sensor reaction to ethanol.

We use this observation to convert the scheme in Fig. 2(*a*) to the scheme in Fig. 2(*b*), where the guiding idea is that the sensor is a pure integrator. As we shall see, this modification also works when $\varepsilon > 0$.

4 Slow Sensor and a Static Map

We consider applications in which the goal is to maximize the output of an unknown nonlinear map $f(\theta)$ by varying the input θ. The signal $f(\theta(t))$ is measured through a slow sensor, namely, the signal $\mu(t)$, governed by $\dot{\mu} = -\varepsilon\mu + bf(\theta)$, is measured. Let the maximizing value of θ be denoted as θ^*. We assume that the nonlinear map is quadratic,

$$f(\theta) = f^* - q_\theta(\theta - \theta^*)^2 \tag{2}$$

where besides θ^* and f^* being unknown, q_θ is an unknown positive constant.

In this section, we study the case of a slow sensor ($\varepsilon > 0$ but small). We consider both the ES scheme with a washout filter ($h > 0$) and without a washout filter ($h = 0$). In the next section, we address the same two cases but for a sensor modeled as a pure integrator ($\varepsilon = 0$).

Let $\hat{\theta}$ be the estimate of θ^*, and $\tilde{\theta} = \hat{\theta} - \theta^*$ be the error. From Fig. 2(*b*), we obtain

$$\hat{\theta} = k\left(\eta \sin(\omega t) + \frac{1}{s}[-\eta\omega \cos(\omega t)]\right) \tag{3}$$

Note that we mix the time and frequency domain notation by using the brackets $[\cdot]$ to denote that the transfer function acts as an operator on a time-domain function.

To prove stability, we are going to analyze $\tilde{\theta}$, η, and μ. Assuming the nonlinear map (2) and the block diagram in Fig. 2(*b*), we obtain

$$\mu = \frac{b}{s+\varepsilon}[f^* - q_\theta(\theta - \theta^*)^2] \tag{4}$$

$$\eta = \frac{s}{s+h}[\mu] \tag{5}$$

$$\tilde{\theta} = k\left(\eta \sin(\omega t) + \frac{1}{s}[-\eta\omega \cos(\omega t)]\right) - \theta^* \tag{6}$$

By rearranging Eq. (5), multiplying Eqs. (4) and (6) by s, replacing θ with $\tilde{\theta}$, and setting $\tau = \omega t$, we obtain

$$\frac{d\mu}{d\tau} = \frac{1}{\omega}[bf^* - bq_\theta(\tilde{\theta} + a\sin(\tau))^2 - \varepsilon\mu] \tag{7}$$

$$\frac{d\eta}{d\tau} = \frac{1}{\omega}[bf^* - bq_\theta(\tilde{\theta} + a\sin(\tau))^2 - \varepsilon\mu - h\eta] \tag{8}$$

$$\frac{d\tilde{\theta}}{d\tau} = -\frac{1}{\omega}k(h\eta + \varepsilon\mu - bf^* + bq_\theta(\tilde{\theta} + a\sin(\tau))^2)\sin(\tau) \tag{9}$$

Using the following two identities:

$$\frac{1}{2\pi}\int_0^{2\pi} (\tilde{\theta} + a\sin(\tau))^2 d\tau = \tilde{\theta}^2 + \frac{a^2}{2} \tag{10}$$

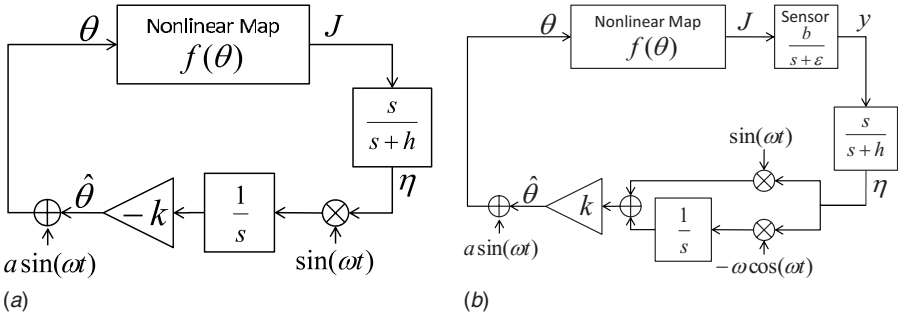

Fig. 2 Extremum seeking block diagrams. The modified extremum seeking algorithm (*b*) applies both to the case with a slow sensor ($\varepsilon > 0$) and to the case with a sensor modeled as a pure integrator, which we also refer to as a "drifting sensor" ($\varepsilon = 0$). In both cases ($\varepsilon > 0$ and $\varepsilon > 0$), the washout filter is optional (both $h > 0$ and $h = 0$ are permissible).

$$\frac{1}{2\pi}\int_0^{2\pi}(\tilde{\theta}+a\sin(\tau))^2\sin(\tau)\mathrm{d}\tau=\tilde{\theta}a \tag{11}$$

to average Eqs. (7)–(9), we obtain

$$\frac{\mathrm{d}\mu_{\mathrm{avg}}}{\mathrm{d}\tau}=\frac{1}{\omega}\left[bf^*-bq_\theta\left(\tilde{\theta}^2+\frac{a^2}{2}\right)-\varepsilon\mu_{\mathrm{avg}}\right] \tag{12}$$

$$\frac{\mathrm{d}\eta_{\mathrm{avg}}}{\mathrm{d}\tau}=\frac{1}{\omega}\left[bf^*-bq_\theta\left(\tilde{\theta}^2+\frac{a^2}{2}\right)-\varepsilon\mu_{\mathrm{avg}}-h\eta_{\mathrm{avg}}\right] \tag{13}$$

$$\frac{\mathrm{d}\tilde{\theta}_{\mathrm{avg}}}{\mathrm{d}\tau}=-\frac{kbaq_\theta}{\omega}\tilde{\theta}_{\mathrm{avg}} \tag{14}$$

The equilibrium of the averaged system (12)–(14) is $[\mu^e_{\mathrm{avg}},\eta^e_{\mathrm{avg}},\tilde{\theta}^e_{\mathrm{avg}}]=[(b/\varepsilon)(f^*+(q_\theta a^2/2)),0,0]$, with the Jacobian of

$$J_{\mathrm{avg}}=\frac{1}{\omega}\begin{bmatrix}-\varepsilon & 0 & 0\\ -\varepsilon & -h & 0\\ 0 & 0 & -kbaq_\theta\end{bmatrix} \tag{15}$$

Given that the nonlinear map has a maximum ($q_\theta>0$) and that the sensor is stable ($\varepsilon>0$) and noninverting ($b>0$), it follows that, if we choose $a,\omega,k,h>0$, the Jacobian (15) is Hurwitz and the equilibrium of the averaged system (12)–(14) is locally exponentially stable. From averaging theorem [20], we get the following result.

THEOREM 1. *There exists ω^* such that for all finite $\omega>\omega^*$, the system in Fig. 2 with nonlinear map (2) has a unique exponentially stable periodic solution $(\mu^{2\pi/\omega}(t),\eta^{2\pi/\omega}(t),\tilde{\theta}^{2\pi/\omega}(t))$ of period $2\pi/\omega$, which satisfies*

$$\left\|\begin{bmatrix}\mu^{2\pi/\omega}(t)-\dfrac{b}{\varepsilon}\left(f^*+\dfrac{q_\theta a^2}{2}\right)\\ \eta^{2\pi/\omega}(t)\\ \tilde{\theta}^{2\pi/\omega}(t)\end{bmatrix}\right\|\le O(1/\omega),\quad \forall\, t\ge 0 \tag{16}$$

Since $\theta-\theta^*=\tilde{\theta}+a\sin(\omega t)=(\tilde{\theta}-\tilde{\theta}^{2\pi/\omega})+\tilde{\theta}^{2\pi/\omega}+a\sin(\omega t)$, the theorem implies that the first term is zero, the second term is $O(1/\omega)$, and the third term is $O(a)$. Thus $\limsup_{t\to\infty}|\theta(t)-\theta^*|=O(1/\omega)$. Hence, we get $\limsup_{t\to\infty}|f(\theta(t))-f^*|=O(a^2+1/\omega^2)$, which characterizes the asymptotic performance of the extremum seeking loop in Fig. 2.

Figure 4 shows the simulations for a moving sensor along the length of a pipe, where the objective is to localize a gas leak on the pipe with the use of sensor-compensated extremum seeking, with the gas distribution, which is shown in Fig. 3, modeled in the form $f(\theta)=\delta^*/1+p_\theta(\theta-\theta^*)^2$, where $\delta^*=250$, $p_\theta=0.5$, and $\theta^*=0$. The extremum seeking parameters were chosen as $\omega=30$, $a=0.2$, $k=10$, and $h=1$. We assume the sensor model (1) with the parameters $\varepsilon=0.046$ and $b=0.037$. Figure 4(*b*) shows the position of the sensor in reference to the gas leak with a starting position of 3. The nonlinear map output (J) and the sensor position (θ) quickly converge to a periodic motion around f^* and θ^*, respectively.

Note in Fig. 4(*d*) that the sensor reading converges very slowly. The time interval for which J and $\hat{\theta}$ are shown in Fig. 4 is only one-tenth of the time interval on which η and y are shown. This is done in order to display the details of the rapidly convergent sensor position $\hat{\theta}$, while the sensor reading y is about ten times slower. More specifically, even though it takes the sensor reading 120 s to settle the extremum seeking algorithm is able to tune $\hat{\theta}$ to achieve maximum output from the nonlinear map in less than 6 s. The convergence would be orders of magnitude slower if the algorithm had to wait for the sensor reading to settle every time it wanted to tweak θ.

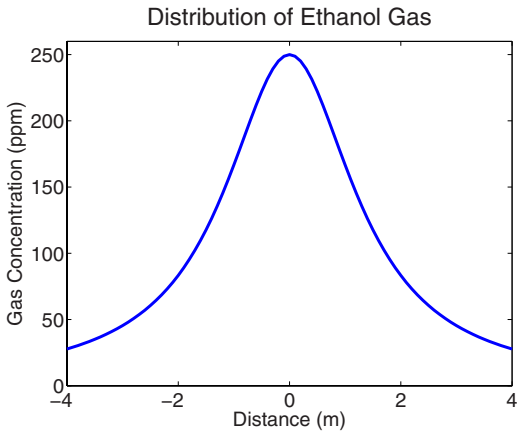

Fig. 3 Gas concentration distribution along the pipe with gas leak at position 0

In some applications, the use of washout filters may be undesirable because they act as approximate differentiators and therefore may result in the amplification of noise. Dropping the washout filter still results in a stable system, namely, the washout filter is used for performance reasons, not for stability reasons or to "cancel" the extremely slow (integratorlike) dynamics of the sensor. The proof for this case (omitted) is very similar to the proof for the case where the sensor is a pure integrator but the ES scheme does employ a washout filter (Theorem 3), with the Jacobian of the averaged system given as

$$J_{\mathrm{avg}}=\frac{1}{\omega}\begin{bmatrix}-\varepsilon & 0\\ 0 & -kbaq_\theta\end{bmatrix} \tag{17}$$

THEOREM 2. *Consider the system in Fig. 2 with the nonlinear map of form (2) and without the washout filter. There exists ω^* such that for all finite $\omega>\omega^*$ the system has a unique exponentially stable periodic solution $(y^{2\pi/\omega}(t),\tilde{\theta}^{2\pi/\omega}(t))$ of period $2\pi/\omega$, which satisfies*

$$\left\|\begin{bmatrix}y^{2\pi/\omega}(t)-\dfrac{b}{\varepsilon}\left(f^*+\dfrac{q_\theta a^2}{2}\right)\\ \tilde{\theta}^{2\pi/\omega}(t)\end{bmatrix}\right\|\le O(1/\omega),\quad \forall\, t\ge 0 \tag{18}$$

Simulation (not included) for the system in Theorem 2 shows convergence rate that is inferior to that of the algorithm with the washout filter (Theorem 1). This convergence rate difference is not captured by the averaging analysis because the approximation accuracy of averaging is low when some of the eigenvalues of the average system are small due to small ε.

5 Drifting Sensor and a Static Map

Our scheme works even when $\varepsilon=0$, namely, when the sensor is a pure integrator. This is a rather extreme situation of a sensor that responds but permanently drifts in its value (toward infinity). All that we can achieve in this case is to maximize the sensor's input, since its output never settles.

The stability analysis for this case mimics some parts of the proof for Theorem 1. Assuming the nonlinear map in Eq. (2) and setting $\varepsilon=0$, we write Eq. (4) as $\mu=b/s[f^*-q_\theta(\tilde{\theta}+a\sin(\omega t))^2]$. Since the sensor output μ is not going to settle when its input $\hat{\theta}$ settles, we do not include the sensor output as a state for which we are proving convergence. Using the identities (10) and (11), we obtain the following averaged equations:

$$\frac{d\eta_{\mathrm{avg}}}{d\tau}=\frac{1}{\omega}\left[bf^*-bq_\theta\left(\tilde{\theta}^2+\frac{a^2}{2}\right)-h\eta_{\mathrm{avg}}\right] \tag{19}$$

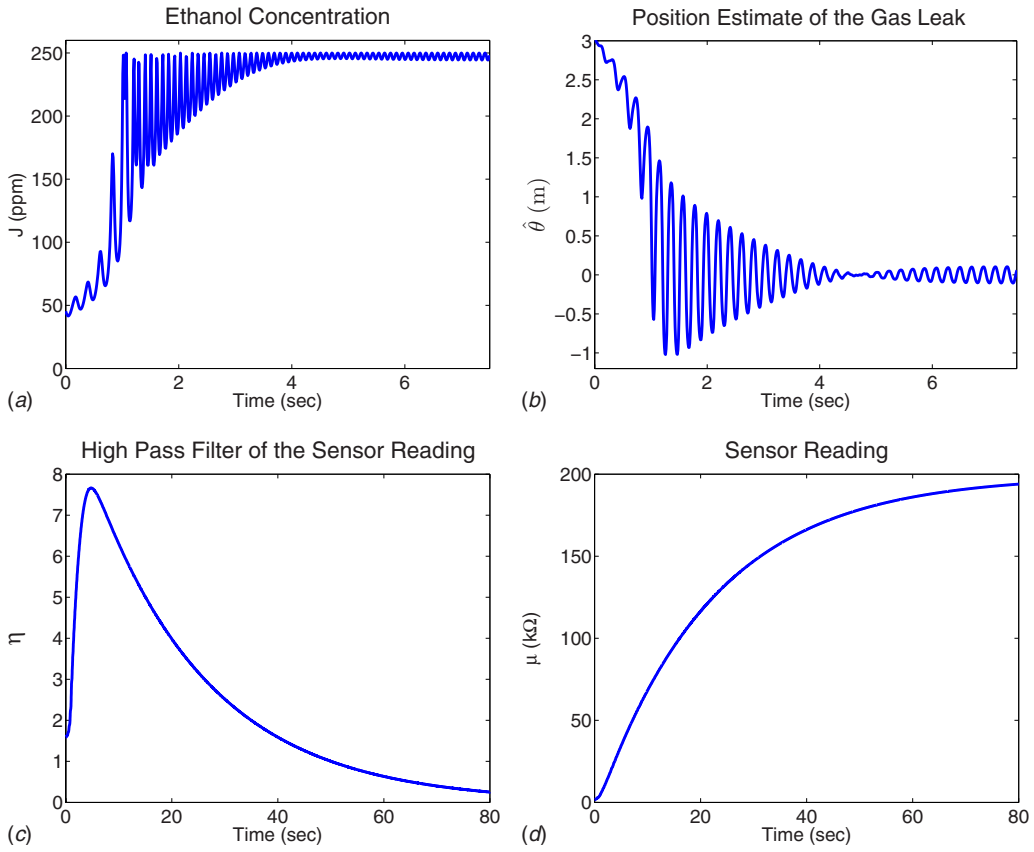

Fig. 4 Simulation results for modified extremum seeking with slow sensor dynamics. (*a*) Output of the nonlinear map. (*b*) The sensor position relative to θ^*. (*c*) The signal after the high pass filter. (*d*) The slow sensor reading.

$$\frac{d\tilde{\theta}_{\text{avg}}}{d\tau} = \frac{1}{\omega}[-kbaq_\theta \tilde{\theta}_{\text{avg}}] \tag{20}$$

The averaged systems (19) and (20) have the equilibrium $[\eta^e_{\text{avg}}, \tilde{\theta}^e_{\text{avg}}] = [(b/h)(f^* + (q_\theta a^2/2)), 0]$, with the Jacobian of

$$J_{\text{avg}} = \frac{1}{\omega}\begin{bmatrix} -h & 0 \\ 0 & -kbaq_\theta \end{bmatrix} \tag{21}$$

THEOREM 3. *There exists ω^* such that for all finite $\omega > \omega^*$, the system in Fig. 2 with the nonlinear map of form (2) and $\varepsilon = 0$ in the sensor dynamics has a unique exponentially stable periodic solution $(\eta^{2\pi/\omega}(t), \tilde{\theta}^{2\pi/\omega}(t))$ of period $2\pi/\omega$, which satisfies*

$$\left\| \begin{bmatrix} \eta^{2\pi/\omega} - \dfrac{b}{h}\left(f^* + \dfrac{q_\theta a^2}{2}\right) \\ \tilde{\theta}^{2\pi/\omega} \end{bmatrix} \right\| \leq O(1/\omega), \quad \forall\, t \geq 0 \tag{22}$$

Figure 5 shows a simulation with a sensor $G_{\text{sensor}}(s) = b/s$, $\theta^* = 0$, $f^* = 1$, $q_\theta = 0.5$, and $b = 1$. The ES parameters are chosen as $\omega = 30$, $a = 0.2$, $k = 10$, and $h = 1$. Figure 5(*a*) shows the ability of the sensor-compensated ES scheme to maximize the output of a nonlinear map even with a marginally stable sensor. Figure 5(*b*) shows $\hat{\theta}$ starting from 3 and converging to a periodic motion around $\theta^* = 0$.

The scheme studied in Theorem 3 contains a cascade of the sensor's integrator dynamics and of a washout filter. It may appear that the key to the result is that a differentiator cancels an integrator. This is not the case at all, as we illustrate with the next simulations, for the system with $G_{\text{sensor}}(s) = b/s$ and without the washout filter (i.e., with $h = 0$). This simple result is given without a proof, which follows from the fact that the (scalar) Jacobian is $-kbaq_\theta/\omega$ (in the τ time scale).

THEOREM 4. *Consider the system in Fig. 2 without the washout filter, with ε set to zero in the sensor dynamics, and the nonlinear map of form (2). There exists ω^* such that for all $\omega > \omega^*$, the system has a unique exponentially stable periodic solution $\tilde{\theta}^{2\pi/\omega}(t)$ of period $2\pi/\omega$, which satisfies $\|\tilde{\theta}^{2\pi/\omega}(t)\| \leq O(1/\omega)$, $\forall\, t \geq 0$.*

Simulation results for the system in Theorem 4 are shown in Fig. 6 for $f^* = 1$, $q_\theta = 0.5$, $b = 1$, $\omega = 30$, $a = 0.2$, $k = 10$, and $h = 1$. As expected, θ and f converge to a periodic motion around θ^* and f^*, respectively. The drifting sensor without the washout filter has significant oscillations after settling compared with the previous case with the washout filter. The significance of the result in Theorem 4, shown in Fig. 6, is that the modified extremum seeking scheme is not merely acting based on the signal trend/derivative rather than on the signal value, which would have been the case if the inclusion of a washout filter had turned out to be crucial. Rather than "canceling" the sensor's integrator, our scheme *leverages* it, by using its presence for the function of tuning of $\hat{\theta}(t)$ in the ES loop.

6 Navigation of a 2D Point Mass With a Slow Sensor

In this section, we study the case of a slow sensor ($\varepsilon > 0$ but small) on a vehicle modeled as a 2D point mass $\dot{x}(t) = u_x(t)$ and $\dot{y}(t) = u_y(t)$, where $u_x(t), u_y(t)$ are two independent velocity inputs to the vehicle. For simplicity of our presentation, we assume that the nonlinear map is quadratic with the form

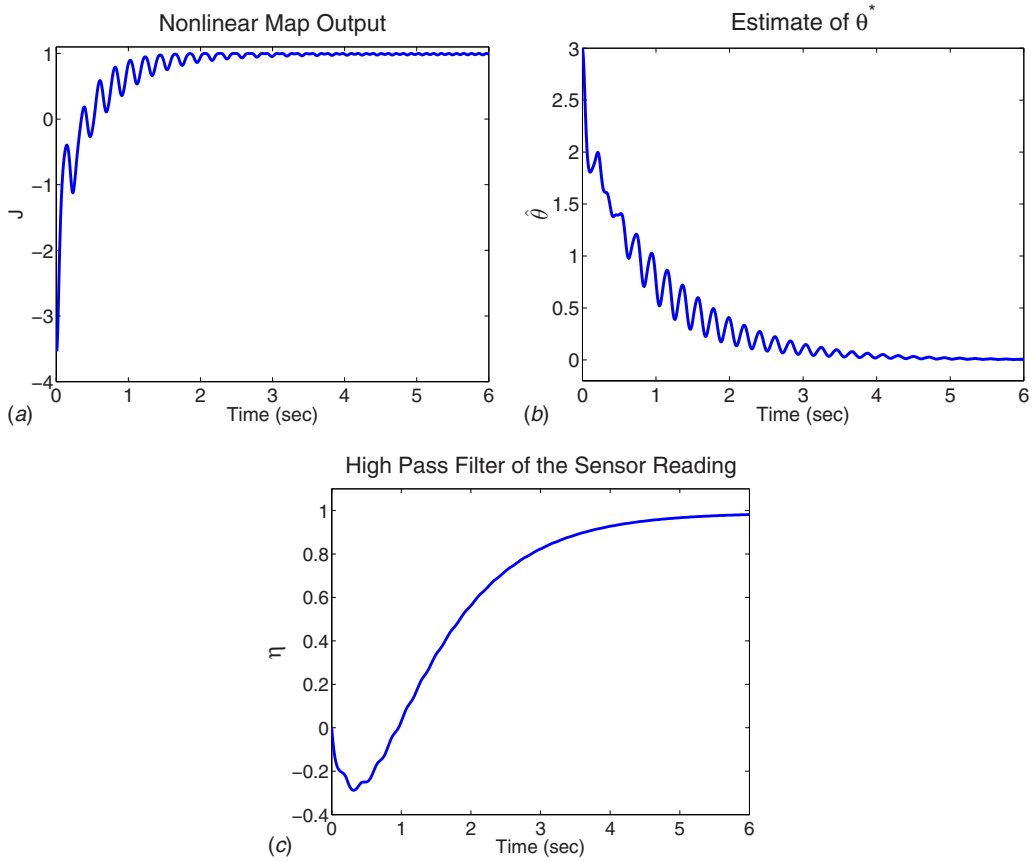

Fig. 5 Simulation results for extremum seeking with $G_{sensor}(s)=b/s$ with washout filter. (*a*) Output of the nonlinear map. (*b*) The sensor position relative to θ^*. (*c*) The signal after the high pass filter.

$$f(x,y) = f^* - q_x(x-x^*)^2 - q_y(y-y^*)^2 \tag{23}$$

where (x^*, y^*) is the maximizer, f^* is the maximum, and q_x, q_y are some unknown positive constants.

We develop a scheme that accounts for the vehicle integrator dynamics in the following manner. We start from the scheme for a static map in Fig. 2. To get an integrator to appear at the input of the nonlinear map, we first place the term $1=s/s$ between the ES gain (k) and the addition of the perturbation $a\sin(\omega t)$. Then, taking the term $1/s$ from the term s/s and moving it downstream the signal flow direction and past the perturbation input, which results in a differentiation of the perturbation, we get an integrator to appear in at the input of the nonlinear map. Then, realizing that a differentiator s, which remains from the term s/s, cannot be implemented, we replace it with an approximate differentiator, i.e., a washout filter $s/(s+d_x)$. Finally, we take advantage of the availability of the integrator in the lowest branch of the extremum seeking loop and, with a suitable block diagram manipulation, arrive at the scheme given in the x-channel of the scheme in Fig. 7.

To go from a 1D scheme to a two-input 2D-navigation scheme,

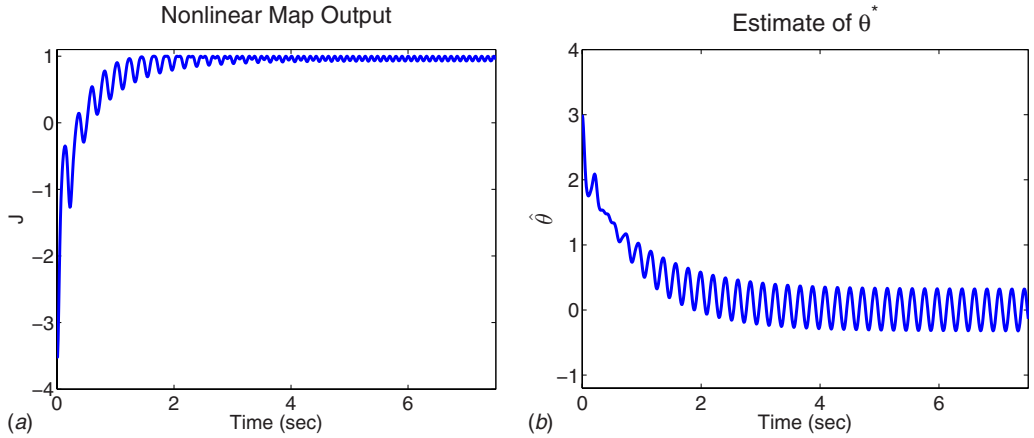

Fig. 6 Simulation results for extremum seeking with $G_{sensor}(s)=b/s$ and without washout filter. (*a*) Output of the nonlinear map. (*b*) The sensor position relative to θ^*.

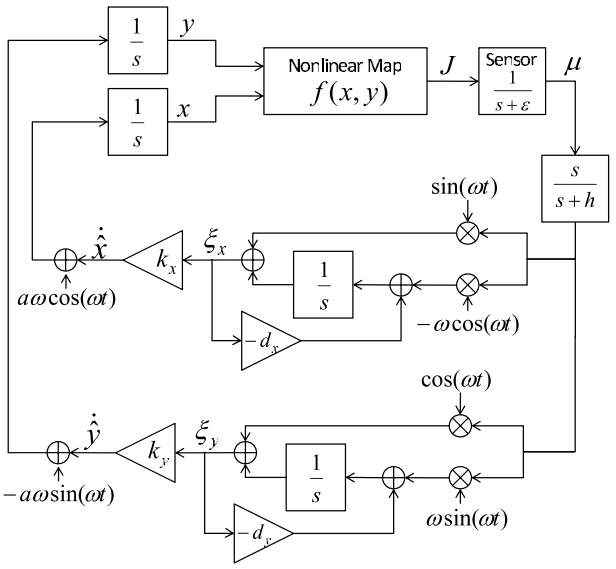

Fig. 7 Modified ES for 2D point mass vehicle with slow sensor. The scheme applies both to the case with a slow sensor ($\varepsilon>0$) and to the case with a sensor modeled as a pure integrator, which we also refer to as a "drifting sensor" ($\varepsilon=0$), and with both $h>0$ and $h=0$ being permissible.

we simply add another extremum seeking channel with the perturbation and the demodulation applied with a 90 deg phase shift, as was done in Ref. [7]. The vehicle control is given by $u_x(t)=a\omega\cos(\omega t)+k_x\xi_x(t)$ and $u_y(t)=-a\omega\sin(\omega t)+k_y\xi_y(t)$.

We introduce the new coordinates $\tilde{x}=x-x^*-a\sin(\omega t)$ and $\tilde{y}=y-y^*-a\cos(\omega t)$. With the new coordinates, the map (23) becomes $f(x,y)=f^*-q_x(\tilde{x}+a\sin(\omega t))^2-q_y(\tilde{y}+a\cos(\omega t))^2$. From the block diagram in Fig. 2(*c*), we write the equations for μ, η, ξ_x, and ξ_y,

$$\mu=\frac{b}{s+\varepsilon}[f^*-q_x(x-x^*)^2-q_y(y-y^*)^2] \tag{24}$$

$$\eta=\frac{s}{s+h}[\mu] \tag{25}$$

$$\xi_x=\eta\sin(\omega t)-\frac{1}{s}[\eta\omega\cos(\omega t)+d_x\xi_x] \tag{26}$$

$$\xi_y=\eta\cos(\omega t)+\frac{1}{s}[\eta\omega\sin(\omega t)-d_y\xi_y] \tag{27}$$

By replacing (x,y) with $(\tilde{x},\tilde{y})$, letting $\tau=\omega t$, and using Eqs. (10) and (11) to average, we obtain

$$\frac{d\mu_{avg}}{d\tau}=\frac{1}{\omega}\left[-\varepsilon\mu_{avg}+bf^*-bq_x\left(\tilde{x}_{avg}^2+\frac{a^2}{2}\right)-bq_y\left(\tilde{y}_{avg}^2+\frac{a^2}{2}\right)\right] \tag{28}$$

$$\frac{d\eta_{avg}}{d\tau}=\frac{1}{\omega}\left[-h\eta-\varepsilon\mu_{avg}+bf^*-bq_x\left(\tilde{x}_{avg}^2+\frac{a^2}{2}\right)-bq_y\left(\tilde{y}_{avg}^2+\frac{a^2}{2}\right)\right] \tag{29}$$

$$\frac{d\xi_{x\,avg}}{d\tau}=-\frac{1}{\omega}(baq_x\tilde{x}_{avg}+d_x\xi_{x\,avg}) \tag{30}$$

$$\frac{d\tilde{x}_{avg}}{d\tau}=\frac{k_x}{\omega}\xi_{x\,avg} \tag{31}$$

$$\frac{d\xi_{y\,avg}}{d\tau}=-\frac{1}{\omega}(baq_y\tilde{y}_{avg}+d_y\xi_{y\,avg}) \tag{32}$$

$$\frac{d\tilde{y}_{avg}}{d\tau}=\frac{k_y}{\omega}\xi_{y\,avg} \tag{33}$$

The equilibrium of the averaged system (28)–(33) is $[\mu_{avg}^e,\eta_{avg}^e,\xi_{x\,avg}^e,\tilde{x}_{avg}^e,\xi_{y\,avg}^e,\tilde{y}_{avg}^e]=[(b/\varepsilon)(f^*+((q_x+q_y)a^2/2)),0,0,0,0,0]$, with the Jacobian

$$J_{avg}=\frac{1}{\omega}\begin{bmatrix}-\varepsilon & 0 & 0 & 0 & 0 & 0\\ -\varepsilon & -h & 0 & 0 & 0 & 0\\ 0 & 0 & -d_x & -baq_x & 0 & 0\\ 0 & 0 & k_x & 0 & 0 & 0\\ 0 & 0 & 0 & 0 & -d_y & -baq_x\\ 0 & 0 & 0 & 0 & k_y & 0\end{bmatrix} \tag{34}$$

Given that $q_x,q_y>0,\varepsilon>0$ and $b>0$, it follows that, if we choose $a,\omega,k_x,k_y,d_x,d_y,h>0$, the Jacobian (34) is Hurwitz and the equilibrium of the averaged system (28)–(33) is locally exponentially stable. From averaging theorem [20], we get the following result.

THEOREM 5. *There exists ω^* such that for all finite $\omega>\omega^*$, the system in Fig. 2(c) with nonlinear map (23) has a unique exponentially stable periodic solution $(\mu^{2\pi/\omega}(t),\eta^{2\pi/\omega}(t),\xi_x^{2\pi/\omega}(t),\tilde{x}^{2\pi/\omega}(t),\xi_y^{2\pi/\omega}(t),\tilde{y}^{2\pi/\omega}(t))$ of period $2\pi/\omega$, which satisfies*

$$\left\|\begin{bmatrix}\mu^{2\pi/\omega}(t)-\dfrac{b}{\varepsilon}\left(f^*+\dfrac{(q_x+q_y)a^2}{2}\right)\\ \eta^{2\pi/\omega}(t)\\ \xi_x^{2\pi/\omega}(t)\\ \tilde{x}^{2\pi/\omega}(t)\\ \xi_y^{2\pi/\omega}(t)\\ \tilde{y}^{2\pi/\omega}(t)\end{bmatrix}\right\|\le O(1/\omega),\quad\forall\, t\ge 0 \tag{35}$$

Since $x-x^*=\tilde{x}+a\sin(\omega t)=(\tilde{x}-\tilde{x}^{2\pi/\omega})+\tilde{x}^{2\pi/\omega}+a\sin(\omega t)$, the theorem implies that the first term is zero, the second term is $O(1/\omega)$, and the third term is $O(a)$. Thus $\limsup_{t\to\infty}|x(t)-x^*|=O(1/\omega)+O(a)$. Similarly in y, we obtain $\limsup_{t\to\infty}|y(t)-y^*|=O(1/\omega)+O(a)$. Hence, we get $\limsup_{t\to\infty}|f(x(t),y(t))-f^*|=O(a^2+1/\omega^2)$, which characterizes the asymptotic performance of the extremum seeking loop in Fig. 7.

Figure 8 shows the simulations of a point mass vehicle starting at position (1,1) with a slow sensor dynamics using actuator-sensor-compensated extremum seeking on a nonlinear map modeled in the form $f(x,y)=\delta^*/(1+p_x(x-x^*)^2+p_y(y-y^*)^2)$, where $\delta^*=250$, $p_x=1$, $p_y=0.5$, and $(x^*,y^*)=(0,0)$. The extremum seeking parameters are $\omega=20$, $a=0.5$, $k_x=1$, $k_y=1$, $d_x=0.2$, $d_y=0.2$, and $h=1$. We assume the sensor model (1) with the parameters $\varepsilon=0.046$ and $b=0.037$. It is interesting to note that the time it takes the vehicle to settle to the location of the maximum concentration is one-fourth the time that it takes the sensor reading to settle. The increase in convergence time of the position of the sensor from the previous 1D case to the 2D case is mainly due to the addition of the actuator dynamics for the vehicle.

Similar to the modified one-dimensional case, the two dimensional modified extremum seeking case with point mass actuator dynamics can be extended to the two dimensional case with no washout filter or with a purely drifting sensor.

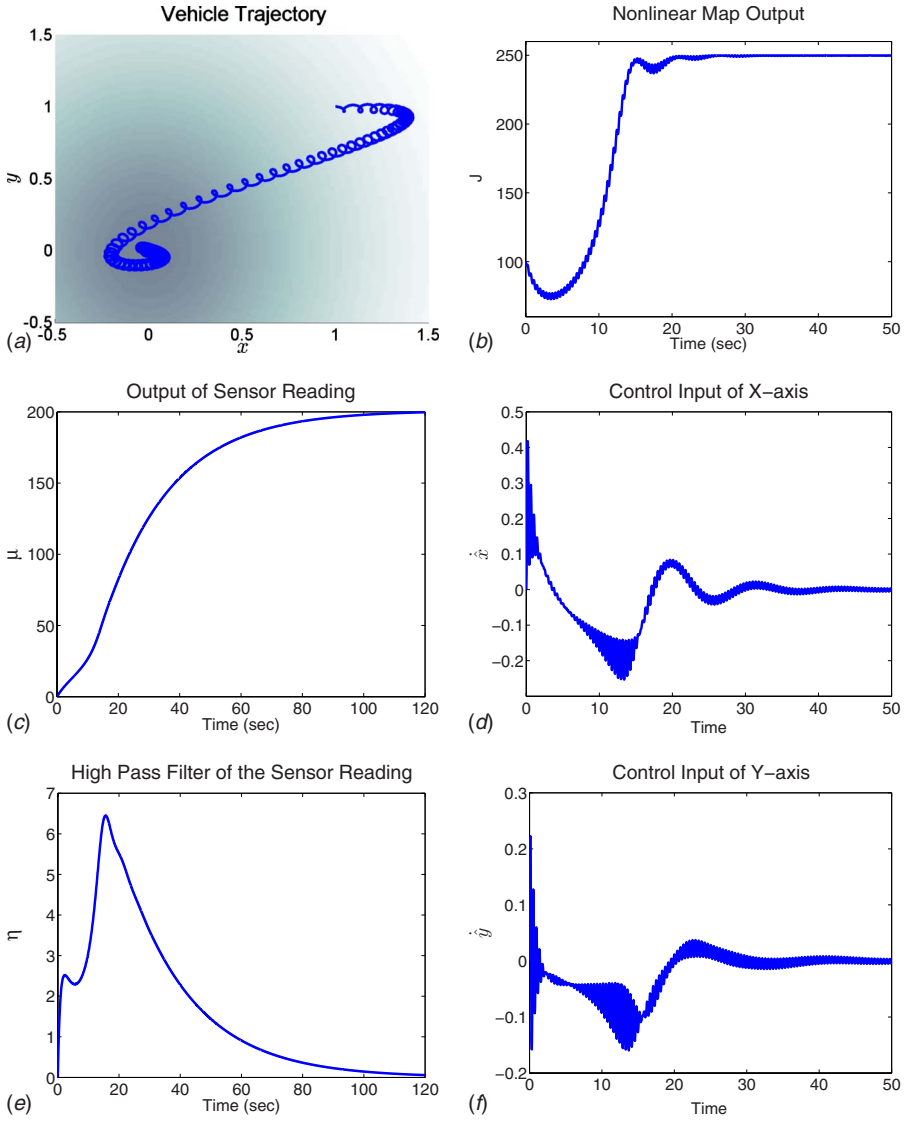

Fig. 8 Simulation results for extremum seeking on a 2D point mass with a slow sensor. (*a*) Vehicle trajectory with the intensity of the nonlinear map in the background. (*b*) Output of the nonlinear map. (*c*) The slow sensor output. (*e*) The output of the washout filter. ((*d*) and (*f*)) The control input of *x*-axis and *y*-axis before the addition of the perturbation, respectively.

Acknowledgment

The authors gratefully acknowledge the contribution of Alexander Vergara and Kerem Muezzinoglu for their helpful knowledge of the metal oxide sensors, and the funding support by the NSF Grant No. CMMI-0653834 and by the ONR Grant No. N00014-07-1-0741.

References

[1] Centioli, C., Iannone, F., Mazza, G., Panella, M., Pangione, L., Podda, S., Tuccillo, A., Vitale, V., and Zaccarian, L., 2008, "Maximization of the Lower Hybrid Power Coupling in the Frascati Tokamak Upgrade via Extremum Seeking," Control Eng. Pract., **16**(12), pp. 1468–1478.

[2] Becker, R., King, R., Petz, R., and Nitsche, W., 2007, "Adaptive Closed-Loop Separation Control on a High-Lift Configuration Using Extremum Seeking," AIAA J., **45**(6), pp. 1382–1392.

[3] Li, Y., Rotea, A., Chiu, G. T.-C., Mongeau, L., and Paek, I.-S., 2005, "Extremum Seeking Control of a Tunable Thermoacoustic Cooler," IEEE Trans. Control Syst. Technol., **13**, pp. 527–536.

[4] Stankovic, M. S., and Stipanovic, D., 2009, "Stochastic Extremum Seeking With Applications to Mobile Sensor Networks," American Control Conference.

[5] Tan, Y., Nesic, D., and Mareels, I. M. Y., 2006, "On Non-Local Stability Properties of Extremum Seeking Controllers," Automatica, **42**, pp. 889–903.

[6] Tanelli, M., Astolfi, A., and Savaresi, S., 2006, "Non-Local Extremum Seeking Control for Active Braking Control Systems," Conference on Control Applications.

[7] Zhang, C., Siranosian, A., and Krstic, M., 2007, "Extremum Seeking for Moderately Unstable Systems and for Autonomous Vehicle Target Tracking Without Position Measurements," Automatica, **43**, pp. 1832–1839.

[8] Zhang, C., Arnold, D., Ghods, N., Siranosian, A., and Krstic, M., 2007, "Source Seeking With Nonholonomic Unicycle Without Position Measurement and With Tuning of Forward Velocity," Syst. Control Lett., **56**, pp. 245–252.

[9] Cochran, J., and Krstic, M., 2009, "Nonholonomic Source Seeking With Tuning of Angular Velocity," IEEE Trans. Autom. Control, **54**(4), pp. 717–731.

[10] Ariyur, K. B., and Krstic, M., 2003, *Real Time Optimization by Extremum Seeking Control*, Wiley-Interscience, New York.

[11] Ishida, H., Nakamoto, T., Moriizumi, T., Kikas, T., and Janata, J., 2001, "Plumetracking Robots: A New Application of Chemical Sensors," Biol. Bull., **200**, pp. 222–226.

[12] Ishida, H., Nakayama, G., Nakamoto, T., and Moriizum, T., 1996, "Odor-Source Localization in the Clean Room by an Autonomous Mobile Sensing System," Sens. Actuators B, **33**(1–3), pp. 115–121.

[13] Ishida, H., Nakayama, G., Nakamoto, T., and Moriizum, T., 2002, "Controlling a Gas/Odor Plume-Tracking Robot Based on Transient Responses of Gas Sensors," Proc. IEEE, **2**, pp. 1665–1670.

[14] Belanger, J., and Arbas, E., 1998, "Behavioral Strategies Underlying Pheromone-Modulated Flight in Moths: Lessons From Simulation Studies," J.

Comp. Physiol. [A], **183**(3), pp. 345–360.
[15] Kanzaki, R., 1998, "Coordination of Wing Motion and Walking Suggests Common Control of Zigzag Motor Program in a Male Silkworm Moth," Sensory, Neural, and Behavioral Physiology, **182**(3), pp. 267–276.
[16] Kanzaki, R., Sugi, N., and Shibuya, T., 1992, "Self-Generated Zigzag Turning of Bombyx Mori Males During Pheromonemediated Upwind Walking," Zoolog Sci., **9**(3), pp. 515–527.
[17] Fort, A., Mugnaini, M., Rocchi, S., Serrano-Santos, M., Vignoli, V., and Spinicci, R., 2007, "Simplified Models for SnO_2 Sensors During Chemical and Thermal Transients in Mixtures of Inert, Oxidizing and Reducing Gases," Sens. Actuators B, **124**(1), pp. 245–259.
[18] Fort, A., Rocchi, S., Serrano-Santos, M., Spinicci, R., and Vignoli, V., 2006, "Surface State Model for Conductance Responses During Thermal-Modulation of SnO_2-Based Thick Film Sensors: Part I—Model Derivation," IEEE Trans. Instrum. Meas., **55**(6), pp. 2102–2106.
[19] Fort, A., Mugnaini, M., Rocchi, S., Serrano-Santos, M., Spinicci, R., and Vignoli, V., 2006, "Surface State Model for Conductance Responses During Thermal-Modulation of SnO_2-Based Thick Film Sensors: Part II—Experimental Verification," IEEE Trans. Instrum. Meas., **55**(6), pp. 2107–2117.
[20] Khalil, H., 2002, *Nonlinear Systems*, Prentice-Hall, Englewood Cliffs, NJ.